Available online at www.sciencedirect.com
SCIENCE DIRECT
Polymer 46 (2005) 9831–9839
polymer
www.elsevier.com/locate/polymer

Non-isothermal crystallization of a vinyl alcohol–ethylene copolymer studied by DSC and real time WAXS/SAXS scattering

Manya Krasteva[a], María L. Cerrada[b,*], Rosario Benavente[b], Ernesto Pérez[b]

[a]*Department of General Physics, Physical Faculty, University of Sofia, 5 James Borchier' blvd, 1164 Sofia, Bulgaria*
[b]*Instituto de Ciencia y Tecnología de Polímeros, C/Juan de la Cierva 3, 28006 Madrid, Spain*

Received 26 August 2004; received in revised form 21 April 2005; accepted 11 August 2005
Available online 15 September 2005

Abstract

Time resolved SAXS/WAXS experiments, employing synchrotron radiation, together with DSC studies have been carried out on a vinyl alcohol–ethylene copolymer in order to clarify the morphological changes occurring during the non-isothermal crystallization of that copolymer from the melt. It was found that the SAXS long spacing and the WAXS diffraction peaks appear at the same temperature, revealing that the predominant growth mechanism of this process is nucleation and crystal growth but not density fluctuations. Moreover, the temperature variation of different structural parameters (peaks intensity, degree of crystallinity, long period, lamellar thickness) was comprehensively analyzed. Three temperature intervals are observed in this analysis, which have been interpreted as 'high-temperature crystallization', 'low temperature crystallization' and sub-glass region in order of decreasing temperatures.

Keywords: Vinyl alcohol–ethylene copolymer; Real-time X-ray analysis; Non-isothermal crystallization

1. Introduction

Poly(vinyl alcohol), PVAL, basically consists of hydrophobic (CH_2) and hydrophilic (OH) groups and is one of the polymers that exhibits excellent gas and odor barrier properties, which makes it one of the best material for packaging of sensitive to oxygen products. However, its melting point is close to its heat degradation temperature, then its processing becomes hindered. One way to reduce its melting point is by copolymerization with appropriate comonomers. Introduction of comonomer units usually causes the reduction of the degree of crystallinity and, consequently, leads to a decrease of barrier properties. However, the copolymerization of vinyl acetate and ethylene (E), followed by the subsequent hydrolysis of the acetate groups, leads to the production of vinyl alcohol–ethylene, VAE, copolymers that are crystalline irrespectively of composition. In addition, its degree of crystallinity [1–5] does not change significantly and, therefore, a good balance [6] between barrier properties and moldability is reached in these VAE copolymers with an ethylene content ranging from 28 to 44 mol%.

The commercial PVAL homopolymer is atactic but can easily crystallize in a monoclinic lattice ($a=7.81$ Å, $b=2.52$ Å, $c=5.51$ Å, $\beta=91.7°$), where the polymer chains lay along the *b*-axis of the unit cell [7]. Bunn suggested two intermolecular hydrogen bonding directions, but recent modeling studies have shown that intramolecular bonding is also present [8]. It was found that lattice parameters (*a*, *c*) perpendicular to the molecular axes (*b*) decreased when the annealing temperature increased and an enhancement in crystal perfection took place [9].

The existence of three types of crystalline lattices depending on the composition of VAE copolymers have been proposed: Monoclinic for compositions of 100–60 mol% vinyl alcohol, VAL, pseudohexagonal in the composition range of 60–20 mol% VAL and orthorhombic for 20–0 mol% VAL [3,4]. Later on, studies based on WAXS and DSC showed that both copolymer composition and thermal history determined the crystal structure of these copolymers [5,10]. Other comprehensive crystallographic investigation of highly oriented and well crystallized VAE copolymers with broad range of comonomer content

* Corresponding author. Tel.: +34 91 5622900; fax: 34 91 5644853.
E-mail address: mlcerrada@ictp.csic.es (M.L. Cerrada).

0032-3861/$ - see front matter © 2005 Elsevier Ltd. All rights reserved.
doi:10.1016/j.polymer.2005.08.054

revealed that all the VAE copolymers could crystallize and the crystal structure changed continuously with the copolymer composition [11]. Those authors considered that the continuous changes seemed to come from disordered packing structure, consisted of a random arrangement of E and VAL units. A boundary of crystal structure transformation from PVAL to PE type has been found to be located between 27 and 14 mol% VAL since the crystallographic data in this range can be interpreted equally on the basis of both types of structural models. The structural changes were supposed to probably be due to the smooth variation of setting angle of the zigzag chains, because of changing of direction and quantity of intermolecular hydrogen bonds [11]. The VAL content in crystal lattice was found to be essentially equal to that of the bulk sample, i.e. the crystallization includes with the same probability E as well as VAL entities independently of composition. However, the molecular arrangements were much more disordered within crystalline phase in copolymers than those exhibited in the corresponding homopolymers [12].

Additionally, some studies concerning viscoelastic [13–16], mechanical [17–20] and barrier properties [6,21] of VAE copolymers have been already published. However, an investigation about structure formation during their rapid solidification process is practically absent in the literature. This analysis is of an extraordinary significance because of their important industrial applicability as gas and odor barrier material for packaging and because of the processing conditions imposed for such applications consist of a rapid quenching, similar to that used in the present investigation.

The aim of this work is, therefore, to clarify in more detail the morphological changes occurred in a VAE copolymer during its non-isothermal crystallization from the melt applying a fast cooling rate. Time-resolved SAXS/WAXS as well as DSC studies were used for this purpose. Our attention has been specially focused on the analysis of the structural information that could be derived from one-dimensional correlation function and interface distribution function (IDF).

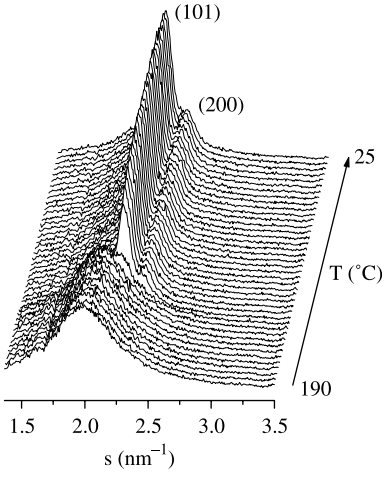

Fig. 1. WAXS patterns of the VAE copolymer cooled from the melt at 12 °C/min. For clarity, only one every two frames have been plotted.

2. Experimental

2.1. Materials

A commercially available random VAE copolymer (from Du Pont) was used. The composition in vinyl alcohol determined by means of ^{1}H and ^{13}C NMR spectroscopies is 61 and 62 mol%, respectively. Its density is 1.150 g/cm^3 and its melt flow index 16.0 (g/10 min). Sheet specimens were obtained as films by compression molding in a Collin press between hot plates (210 °C) at a pressure of 2.5 MPa for 8 min. A fast cooling was applied from the molten state to room temperature between plates cooled with water in the press. Thickness of such films ranged from 200 to 250 μm.

2.2. Methods

DSC measurements were carried out in a Perkin–Elmer DSC7 apparatus. Both cooling and heating experiments were performed at a scanning rate of 12 °C/min, the same as in real-time X-ray experiment.

Wide- (WAXS) and small-angle X-ray (SAXS) diffraction patterns were recorded in the transmission mode in the beamline A2 at HASYLAB (Hamburg, Germany) employing synchrotron radiation (with $\lambda = 0.150$ nm). WAXS and SAXS profiles were acquired simultaneously during cooling or heating experiments, similar to those of the DSC, in time frames of 10 s. Two linear position-sensitive detectors were used. The WAXS one, at a distance of around 17 cm from the sample, was calibrated with the different diffractions of a crystalline PET sample, and it was found to cover the spacing ranged from 0.3 to 0.9 nm. The SAXS detector, at a distance of around 200 cm from the sample, was calibrated with the different orders of rat-tail cornea ($L = 65$ nm), and it was found to cover a spacing interval from 5.5 to 50 nm. The diffraction profiles were normalized to the beam intensity and corrected related to an empty sample background and also for the detector's efficiency.

In order to study in detail the structural changes during the non-isothermal crystallization and subsequent melting, the standard Gaussian peak-fitting routine was applied in WAXS spectra. From WAXS measurements (Fig. 1), the temperature dependencies of the d-spacing, d_{hkl}, and their integrated intensity, I_{hkl}, were determined. Moreover, the domain dimensions in the direction perpendicular to the (hkl) planes, L_{hkl}, were obtained from the Scherrer's formula:

$$L_{hkl} = \frac{1}{\delta s_{hkl}} \quad (1)$$

where δs_{hkl} is the full width at half maximum (FHWM) of the corresponding peak.

Long periods were determined from the position of the peak maximum in Lorentz corrected SAXS patterns, L_B, (Fig. 2) as well as from the first maximum after auto-correlation triangle of the normalized one-dimensional correlation function, $\gamma_1(x)$, (Fig. 3(a)) calculated according to the equation [22–24]:

$$\gamma_1(x) = \frac{\int_0^\infty s^2 I(s)\cos(2\pi x s)\mathrm{d}s}{\int_0^\infty s^2 I(s)\mathrm{d}s} \tag{2}$$

where $s = 2\sin\theta/\lambda$ and $I(s)$ is smoothed and corrected for background SAXS intensity, obtained after subtraction of the diffuse scattering in the isotropic state at high temperature. It was found that $I(s)$ obeys the law [25] in the Porod's region:

$$I(s) = I_b + \frac{K}{s^n} \tag{3}$$

where I_b is the background intensity, K is a constant and n was found to be near to 4 for all frames with a good agreement with Porod's law. I_b was determined according to Eq. (3). The extrapolation of SAXS intensity to zero at high s values was made with the same function, whose parameters were separately calculated for each frame and linear extrapolation to zero s value was applied.

The following structural parameters were determined from the analysis of the correlation function [22,23]: (1) The long period, L_γ (Fig. 3(a)); (2) the degree of crystallinity within the stacks of lamella, X_c^{SAXS}; (3) the crystalline lamellar, l_c, and the amorphous layer thickness, l_a, according to the relationships [23] (Fig. 3(a)):

$$X_c^{SAXS}(1 - X_c^{SAXS})L_\gamma = A \tag{4a}$$

$$X_c^{SAXS} L_\gamma = l_c \tag{4b}$$

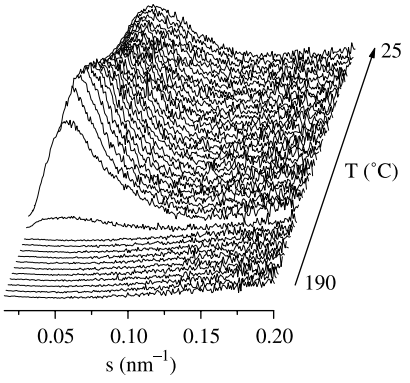

Fig. 2. SAXS curves of the VAE copolymer after subtraction of liquid-like scattering and Lorentz correction. Cooling rate 12 °C/min. For clarity, only one every two frames has been plotted.

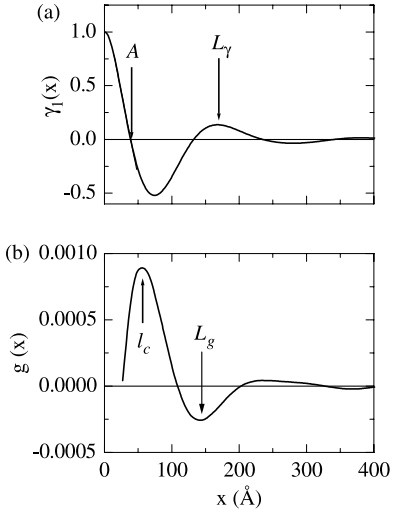

Fig. 3. (a) One-dimensional normalized correlation function and (b) interface distribution function, calculated for $T = 110$ °C.

where A is the intersection of the linear regression to the auto-correlation triangle (LRACT) with the x axis; (4) Porod's invariant in arbitrary units, Q, measured from the non-normalized correlation function, $K(x)$ at $x = 0$ (numerator in Eq. (2)), and Q_{id}, calculated from LRACT to $x = 0$ of $K(x)$ in the auto-correlation triangle. Crystalline lamellar thickness and long period were determined also from the interface distribution function, calculated from the second derivation of $\gamma_1(x)$ (Fig. 3(b)) [26–29]:

$$g(x) = \gamma_1''(x) \tag{5}$$

Lamellar thickness was determined by the position of the first maximum of $g(x)$ and long period from the position of the first minimum.

3. Results

The WAXS and SAXS patterns for the VAE sample on cooling from the melt are shown in Figs. 1 and 2, respectively. Both SAXS long periodicity peak as well as crystal diffractions appear simultaneously at 144 °C and within a short temperature interval they reach their maximum values. This feature is an indication that the process of early stages of crystallization is controlled in this VAE copolymer by nucleation and crystal growth but not by spinodal decomposition [30–33] at least in the limit of time resolution in this experiment.

The WAXS curves are typical for orthorhombic-like crystal lattice in VAE copolymers of similar composition and quenched from the melt. Previous results [5,11] showed that a monoclinic unit cell was observed for VAL contents higher than around 60 mol%, although the monoclinic angle was also clearly dependent on the crystallization conditions, diminishing and approaching the value of 90° for fast cooling rates. Therefore, the present VAE sample, with

a nominal 56 mol% VAL, develops an orthorhombic-like structure under usual crystallization conditions (though a monoclinic unit cell might be obtained for very slow cooling rates, or higher crystallization temperatures).

The temperature dependence of the parameters determined by the analysis of two strongest peaks, diffractions 101 and 200, are shown in Figs. 4 and 5, respectively. The thermal expansion coefficients of d_{101} (corresponding to the d_{110} of PE orthorhombic crystal lattice) is $\beta_T^{(101)} = \mathrm{d}(d_{101})/\mathrm{d}T = (4.24 \pm 0.09) \times 10^{-5}$ nm/deg and $\beta_T^{(200)} = (6.2 \pm 0.2) \times 10^{-5}$ nm/deg. The value of β for both d-spacings changes abruptly at 120 °C (Figs. 4(b) and 5(b)). The jump of the value of thermal expansion coefficient was previously observed for PVAL [8,34]. It was usually associated with appearance of rotational freedom of polymer chains in crystal phase (kink defects). In this latest paper [34], the influence of tacticity of PVAL on thermal motion within crystal phase was examined by WAXS and IR spectroscopy. Authors found the same transition at 120 °C for samples with the smallest content of syndiotactic units and they explained this observation by occurrence of incoherent molecular motion within the crystal regions for those specimens above that temperature. According to them, the intermolecular hydrogen bonds decrease with diminishment of syndiotactic units, which enhance the molecular mobility. Assender et al. [8] supposed two mechanisms of increasing of chain mobility in crystalline regions of PVAL at a particular temperature: kink defects and breaking the hydrogen bonds with increasing temperature. They considered the second one as the most important mechanism. The relative low degree of crystallinity of our sample and, consequently, its low peaks resolution does not allow us to analyze the problem in detail.

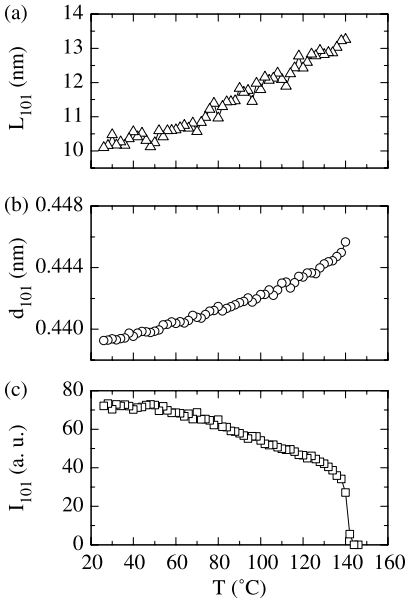

Fig. 4. Results from the analysis of the WAXS patterns in Fig. 1 for peak (101): (a) Crystal domain dimensions in direction perpendicular to the (101) planes; (b) d-spacing; (c) integrated peak intensity.

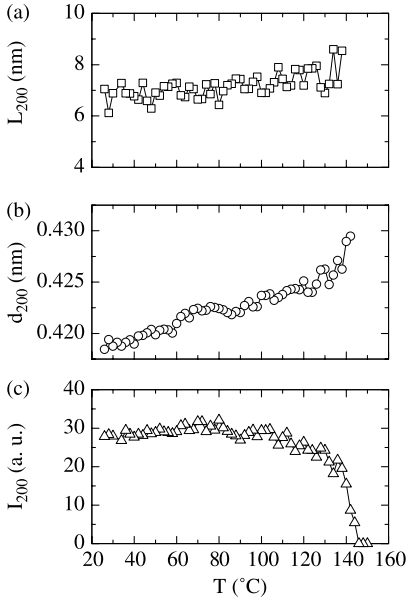

Fig. 5. Results from the analysis of the WAXS patterns in Fig. 1 for peak (200): (a) Crystal domain dimensions in direction perpendicular to the (200) planes; (b) d-spacing; (c) integrated peak intensity.

The results from Gaussian fitting of Lorentz corrected SAXS peak is presented in Fig. 6, while the DSC cooling trace at the same cooling rate (12 °C/min) is depicted in Fig. 7. Three temperature ranges could be clearly distinguished in all of the figures:

(1) The first one goes from the beginning of the crystallization process 144–120 °C. A first stage at around 144–130 °C shows an interval of a rapid increase in the integrated WAXS (Figs. 4(c) and 5(c)) and in SAXS

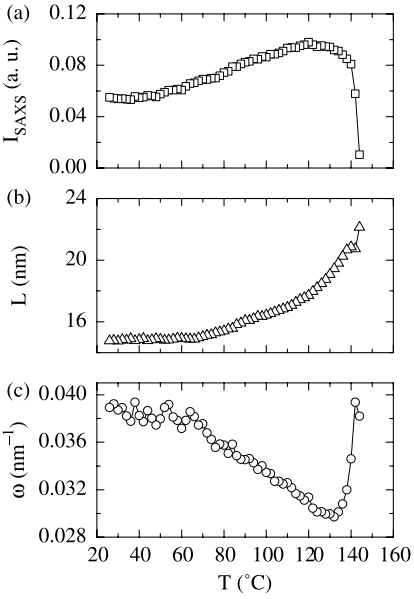

Fig. 6. Results from the Lorentz-corrected SAXS profiles in Fig. 2: (a) integrated SAXS peak intensity; (b) long period, L_B; (c) full width at half maximum, ω.

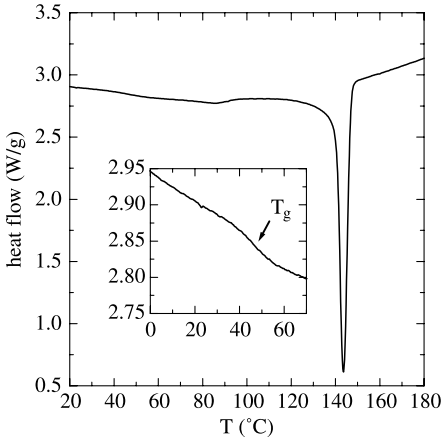

Fig. 7. DSC cooling curve of the VAE copolymer. Cooling rate 12 °C/min.

peaks intensity (Fig. 6(a)) as well as a decrease of FWHM, ω, of SAXS peak (Fig. 6(c)) followed by a second stage ranging between 130 and 120 °C at which SAXS peak intensity passes through a flat maximum and ω through a minimum. This whole region coincides well with the narrow crystallization DSC peak seen in Fig. 7. From these results, we could conclude that the ordering of the crystalline lamellae within the stacks reaches its maximum at the end of this interval since ω is a measure of paracrystalline long-range disorder. In this range, overall degree of crystallinity, calculated by WAXS, reaches a value of around 0.30 (i.e. about 83% of its final value, which is 0.36) (Fig. 8). At the end of this 'high-temperature crystallization process', SAXS degree of crystallinity (0.38) is much higher than overall degree of crystallinity. Therefore, a significant amount of amorphous material outside the lamellar stacks, so called 'amorphous pockets', still exists.

(2) The second interval goes from 120 °C to around 60 °C and is characterized by a continuous smooth rising of WAXS peaks intensity (Figs. 4(c) and 5(c)) that is an evidence of an additional progressive slow crystallization process. The gradual growth of ω (Fig. 6(c)) and decrease of integrated SAXS intensity (Fig. 6(a)) show that the average paracrystalline disorder within the stacks increases. This interval coincides with a broad flat minimum observed in the DSC crystallization curve prolonged up to the onset of the glass transition (inset in Fig. 7).

(3) The third region comprises temperatures ranged from around 60 °C down to the final experimental temperature (27 °C). The beginning of this interval coincides perfectly with the onset of the glass transition temperature (57 °C) determined by DSC [13] in heating experiments. Intensities of WAXS peaks as well as all of the SAXS parameters are constant in this range because of the reduced molecular mobility that hinders the crystallization process. The change of the slope of the crystal coherent length in both crystallographic directions at nearly the same temperature is also in a good agreement with those features just mentioned (Figs. 4(a) and 5(a)).

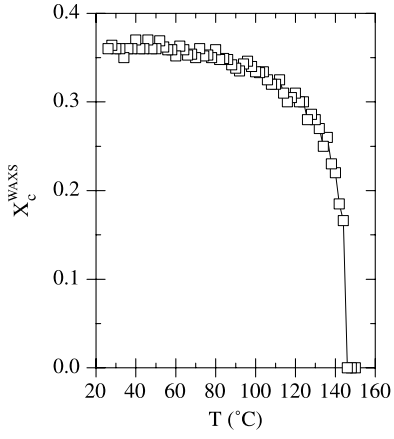

Fig. 8. Variation of the overall degree of crystallinity calculated from the WAXS patterns.

We could conclude from these results described above that the crystallization process passes through two stages: a 'high-temperature crystallization', at which the most perfect and crystallizable chain segments crystallize, and a 'low-temperature crystallization', at which more defect parts of macromolecules form additional more disordered lamellar stacks [27,29,35–38]. The two well-distinguished crystallization regions are typical for polymers with more defect structure of their macromolecules, like copolymers and branched polymers, as LDPE. Therefore, crystallization might be influenced by two factors in this VAE copolymer: polymer main-chain branched structure due to the high-pressure process used during its manufacturing and heterogeneity of copolymer units distribution. On the other hand, as previously reported [11,39], the OH groups even in atactic copolymer are adapted very well into a crystal lattice since the content of OH groups found in the bulk and in crystal phase is the same. LDPE with the analogous main chain structure shows similar results for time-resolved SAXS results than VAE copolymer under study measured at the same conditions (Fig. 9). In LDPE, SAXS peak appears at 87 °C and its intensity smoothly increases down to 57 °C (Fig. 9(c)). However, its SAXS peak width presents an almost constant value in this interval. At lower temperatures ω increases (Fig. 9(b)), whereas L and I_{SAXS} decrease (Fig. 9(a) and (c)). This temperature range is far from LDPE glass transition and, consequently, the third region observed below 60 °C in VAE copolymer cannot be seen. Some differences are worthy to be noticed between both LDPE and VAE polymeric materials: (1) Long period in VAE decreases more sharply during the first crystallization interval than in the secondary one, while the situation is just the opposite in LDPE; (2) the high-temperature crystallization interval is narrower for VAE than for LDPE, because the stronger hydrogen bonds in the former case enhance the crystallization process in

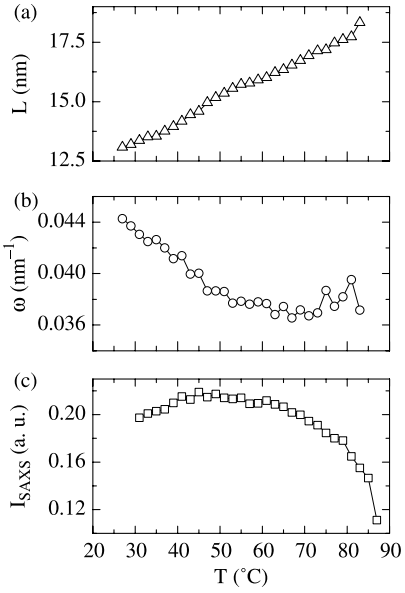

Fig. 9. Results from the Lorentz-corrected SAXS profiles of parent LDPE: (a) Long period, L_B; (b) full width at half maximum, ω; (c) integrated SAXS peak intensity. Cooling rate 12 °C/min.

comparison with the case of LDPE; (3) the initial crystallization temperature is also much higher for VAE (144 °C) than for LDPE (87 °C) because of the higher melting point in the former copolymer due to the inter and intra-hydrogen bonds [4,6,11,40].

In order to obtain a more detail information about the structure within the lamellar stacks, the normalized one-dimensional correlation functions, $\gamma_1(x)$, as well as interface distribution functions (IDF), $g(x)$, were calculated (Fig. 3) [22–24]. Before proceeding to the calculations of $\gamma_1(x)$, a correct determination of the background scattering and an extrapolation of SAXS intensity to the zero intensity at high s values are required. The best non-linear fit for the SAXS curve of the rat-tail calibration sample was that with $R^2 > 0.995$ using the power law expressed by Eq. (3). In the current case, it was not necessary to introduce an artificial interface boundary function [23,27–29,41] because of the good agreement observed with Porod's law. Background, I_b, was subtracted from the initial SAXS curve and the SAXS intensity was extrapolated to zero by using the calculated fit-function (3). Later on, $\gamma_1(x)$ was calculated according to Eq. (2). One example of correlation and IDF is presented in Fig. 3. Both functions are typical for one-dimensional stacks of parallel crystalline lamellae and amorphous layers with paracrystalline periodicity. The long period, L_γ, crystalline lamellar thickness, l_c, amorphous layer thickness, l_a, and degree of crystallinity, X_c^{SAXS}, were determined from the calculated functions according to the Eqs. (4a) and (4b). Degree of crystallinity can be estimated, in principle, from Eq. (4a). However, this equation is quadratic and has two solutions. Consequently, it is not possible to know previously the degree of crystallinity and non-crystal content, unless a certain model or assumption is used. Many authors reported about this uncertainty [27,29,42–46]. The problem is, therefore, to decide if the minor value, for instance, of the two solutions of Eq. (4a) corresponds to the crystal or to the non-crystal content. If the minor phase is chosen as crystalline phase, the calculated degree of crystallinity rapidly increases in the first temperature range, passes through the flat maximum between 135 and 120 °C and gradually decreases down to the onset of glass transition (Fig. 10(b)). The same tendency follows the crystalline lamellar thickness (Fig. 10(a)) and SAXS peak intensity (Fig. 6(a)). At the same time, long period, L_γ, as well as amorphous layer thickness, l_a, rapidly drop down during the first stage of crystallization process, then gradually continue to decrease in the low-temperature crystallization process, and keep constant below the glass transition temperature (Fig. 11). It is reasonable to expect that the more crystallites are generated in the stack, the smaller long period is obtained and the thinner the amorphous layers are. This observation supports our choice of taking the minor component as the crystalline one.

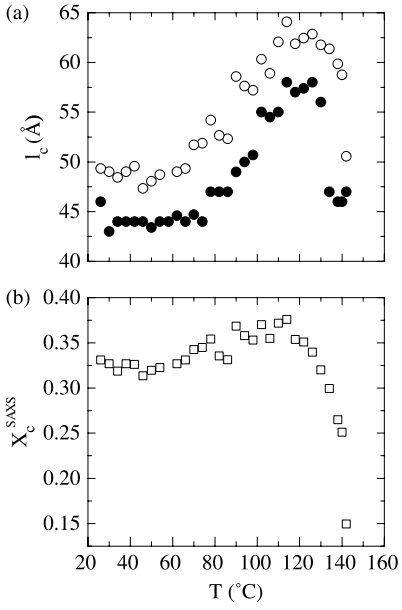

Fig. 10. (a) Crystalline lamellae thickness, l_c, calculated from the one-dimensional correlation function, $\gamma_1(x)$ (open symbols) and from the interface distribution function, $g(x)$ (full symbols), and (b) SAXS degree of crystallinity, calculated from $\gamma_1(x)$, for the VAE copolymer cooled from the melt.

The comparison of the overall degree of crystallinity, evaluated by WAXS (Fig. 8) and crystallinity within the lamellar stacks, calculated by the analysis of correlation functions (Fig. 10(b)) leads us to reach two main conclusions:

(1) The final values of both of them are approximately the same, around 0.35, supporting that the lamellar stacks cover the whole volume of the sample at the end of the crystallization process.

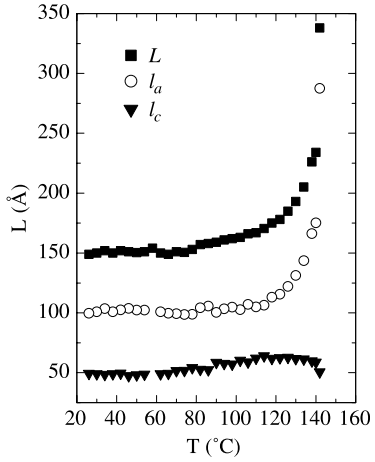

Fig. 11. Parameters calculated from the one-dimensional correlation function, $\gamma_1(x)$, for the VAE copolymer cooled from the melt.

(2) The overall degree of crystallinity increases in both crystallization intervals, although such growth is significantly slower along low-temperature crystallization interval. On the other hand, X_c^{SAXS} passes through a well-expressed maximum just after the end of the first crystallization stage. Consequently, new stacks with thinner crystalline lamellae and lower degree of crystallinity are formed during the low-temperature crystallization process (Fig. 10(a) and (b)).

The depth of the minimum of the IDF, g_{min}, is a sensitive parameter to the number of the stacks [27,28]. Its temperature dependence as well as Porod's invariant, Q, calculated from the numerator of Eq. (2) are presented in Fig. 12(a) and (b), respectively. Q rapidly reaches its maximum value and g_{min} abruptly increases in the first crystallization range. These characteristics point to a process of creation of new stacks as well as new lamellae within the stacks, as is revealed from the rapid decrease of long period (Figs. 6(b) and 11) and amorphous layer thickness (Fig. 11). In the second interval, g_{min} continues its increase that evidences a generation of new stacks within the amorphous regions between primary stacks of more defect macromolecules ('dual-stack model') [27,29,35–38,47,48].

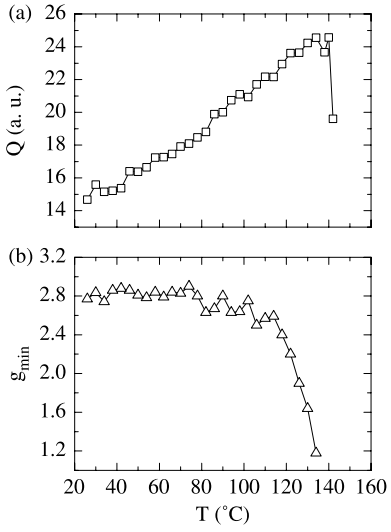

Fig. 12. (a) Invariant of Porod, calculated by the intercept of linear regression to the one dimensional non-normalized correlation function, and (b) absolute value of the depth of the minimum of interface distribution function vs. temperature, for the VAE copolymer cooled from the melt.

There are different methods to determine the long period from SAXS results. Useful conclusions about polymer morphology [28] might be reached by comparison of these different values attained: (i) The Bragg long period, L_B, determined from the position of the Lorentz corrected SAXS curves, usually gives the largest values of L [28]; (ii) the long period determined from the position of first maximum of the correlation function, L_γ, represents the most probable distance between the centers of gravity between two adjacent crystallites; (iii) the long period determined from twice the value of the first minimum of the correlation function, L_γ^m, which is interpreted as a most probable distance between the centers of gravity of a crystal and its adjacent amorphous layer; (iv) the long period determined from the position of the first minimum in the interface distribution function, L_g.

In an ideal periodic structure both values calculated by correlation function should coincide [24]. However, the position of the minimum shifts if the half width of the distribution functions of the layers is different. If the smaller value, l_1, has a broader distribution, the minimum will be shifted to the larger distances, yielding a greater value of L_γ^m and, contrarily, if the distribution of major phase is broader, the minimum will shift to smaller values [28]. Model calculations have shown that the smaller value of L, and closer to the actual one, is that determined from the interface distribution function [28]. Fig. 13 compares the values of long period determined by different methods. All of the results reveal the same temperature tendency. Values

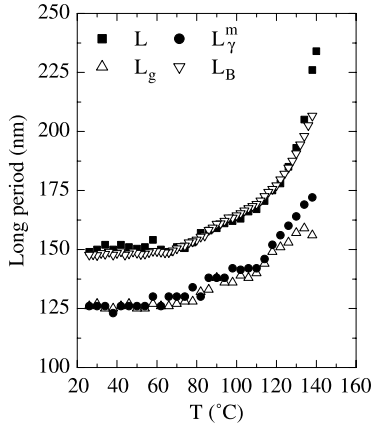

Fig. 13. Temperature dependence of the long period, calculated by different methods, for the VAE copolymer cooled from the melt.

accomplish the following order: $L_B \cong L_\gamma > L_\gamma^m \cong L_g$. Consequently, the major component (in our case the amorphous phase) seems to have a broader distribution than the thickness of crystalline lamellae.

4. Conclusions

(1) Temperature variation of different structural parameters in the conditions of high cooling rates (overall degree of crystallinity, WAXS and SAXS peaks intensity, long period and crystalline lamellae thickness), can be divided in three temperature intervals: 'high temperature crystallization', 'low temperature crystallization' and sub-glass region. The first stage, from 144 °C to around 120 °C, is characterized by fast formation of new stacks as well as new lamellae inside the stacks. It is confirmed by rapid increase of SAXS and WAXS peak intensities, crystal thickness and the overall degree of crystallinity as well as the crystallinity within the lamellar stacks, joined to a diminishment of long period and FWHM of SAXS peak. At the end of this interval a significant amount of amorphous material outside the lamellar stacks, so called 'amorphous pockets', still exists (SAXS degree of crystallinity is much higher than overall degree of crystallinity). Moreover, FWHM reaches its minimum value and SAXS intensity its maximum. Therefore, the stacks with ordered, long periodic structure and more uniform distribution long periodicity, are formed to the end of this stage. The second one takes place from 120 °C to around 60 °C (onset of glass transition). During this temperature range, the overall degree of crystallinity continues increasing but with a slower rate. At the same time, the degree of crystallinity within the lamellar stacks and the most probable value of crystalline lamellar thickness decrease and long period linearly reduces its value. SAXS peak FWHM gradually expands. The number of new stacks, evaluated from the depth of the minimum of the interface distribution function, continues rising although much more slowly. In this stage, more defect crystals and stack structures are generated. At the end of this interval, overall and SAXS degree of crystallinity coincide, i.e. the stacks are filling the whole space of the specimen volume. Finally, the third stage is initiated just below the onset of the glass transition. It is characterized by the constancy of all of the structural parameters, since the crystallization process is hindered because of the lack of molecular mobility.

(2) The crystallization behavior of the VAE copolymer shows the similar features exhibited by one of its parent counterparts, LDPE (although a shift to lower values in the temperature scale is observed for LDPE because of its much lower melting point). The main difference between two polymers is broader temperature interval of the first crystallization range and more smooth transition between two intervals, which is due to the higher crystallization rate of PVAE in comparison with LDPE.

(3) All of the X-ray results were compared with DSC experiments, confirming the main conclusions attained.

(4) Non-isothermal crystallization of the VAE copolymer from the melt leads to the appearance of SAXS and WAXS peaks at the same temperature, revealing that the predominant growth mechanism of this process is nucleation and crystal growth but not density fluctuations.

Acknowledgements

The financial support of Comunidad Autónoma de Madrid, Ministerio de Educación y Ciencia and Comisión Mixta CSIC/Bulgarian Academy of Sciences (Projects 07N/0093/2002, MAT2004-01547 and 2004BG0017, respectively) is gratefully acknowledged. The synchrotron work (in the A2 polymer line of Hasylab at DESY, Hamburg) was supported by the European Community-Research Infrastructure Action under the FP6 'Structuring the European Research Area' Programme (through the Integrated Infrastructure Initiative 'Integrating Activity on Synchrotron and Free Electron Laser Science') (Contract RII3-CT-2004-506008). We thank the collaboration of the Hasylab personnel, specially Dr S. Funari.

References

[1] Bunn CW, Peiser HS. Nature 1947;159:161.
[2] Bodily D, Wunderlich B. J Polym Sci A-2 1966;4:25.
[3] Matsumoto T, Nakamae K, Ogoshi N, Kawasoe M, Oka H. Kobunshi Kagaku 1971;28:610.
[4] Nakamae K, Kameyama M, Matsumoto T. Polym Eng Sci 1979;19:572.
[5] Cerrada ML, Pérez E, Pereña JM, Benavente R. Macromolecules 1998;31:2559.
[6] Finch CA. Polyvinyl alcohol-developments. New York: Wiley; 1992. p. 403.
[7] Bunn CW. Nature 1948;161:929.
[8] Assender HE, Windle AH. Polymer 1998;39:4303.
[9] Assender HE, Windle AH. Polymer 1998;39:4295.
[10] Cerrada ML, Benavente R, Perez E, Pereña JM. Polym J 2000;32:999.
[11] Takahashi M, Tashiro K, Amiya S. Macromolecules 1999;32:5860.
[12] Nishino T, Takano K, Nakamae K. Polymer 1995;36:959.
[13] Cerrada ML, Pereña JM, Benavente R, Pérez E. Polymer 2000;41:6655.
[14] Cerrada ML, Benavente R, Pérez E, Pereña JM. Macromol Chem Phys 2000;201:1858.
[15] Cerrada ML, Benavente R, Pérez E, Pereña JM. J Polym Sci, Part B: Polym Phys 2001;39:1.
[16] Cerrada ML, Benavente R, Pérez E, Pereña JM. Polymer 2001;42:3127.
[17] Djezzar K, Penel L, Lefebvre JM, Seguela R, Germain Y. Polymer 1998;39:3945.

[18] Penel L, Djezzar K, Lefebvre JM, Seguela R, Fontaine H. Polymer 1998;39:4279.
[19] Seguela R, Djezzar K, Penel L, Lefebvre JM, Germain Y. Polymer 1998;40:47.
[20] Seguela R, Djezzar K, Penel L, Lefebvre JM. Polymer 1999;40:2027.
[21] Lagaron JM, Powell AK, Bonner G. Polym Test 2001;20:569.
[22] Vonk CG. Appl Cryst 1973;6:81.
[23] Goderis B, Reynaers H, Koch MHJ, Mathot VBF. J Polym Sci, Part B: Polym Phys 1999;37:1715.
[24] Stroble GR, Schneider M. J Polym Sci, Part B: Polym Phys 1980;18: 1343.
[25] Porod G. In: Glatter O, Kratki O, editors. Small angle X-ray scattering. New York: Academic Press; 1982. p. 17–51 [chapter 2].
[26] Ruland W. Colloid Polym Sci 1977;255:417.
[27] Hsiao BS, Wang Z, Yeh F, Gao Y, Sheth KC. Polymer 1999;40:3515.
[28] Santa Cruz C, Stribeck N, Zachmann HG. Macromolecules 1991;24: 5980.
[29] Denchev Z, Nogales A, Ezquerra TA, Fernandes-Nascimento J, Baltá-Calleja FJ. J Polym Sci, Part B: Polym Phys 2000;38:1167.
[30] Terrill NJ, Fairclough PA, Towns-Andreus E, Komanschek BU, Young RJ, Ryan AJ. Polymer 1998;39:2381.
[31] Wang ZG, Hsiao BS, Sirota ES, Srinivas S. Polymer 2000;41:8825.
[32] Imai M, Mori K, Mizukami T, Kaji K, Kanaya T. Polymer 1992;33: 4451.
[33] Li L, Jeu WH. Macromolecules 2003;36:4862.
[34] Nagura M, Matsuzawa S, Yamaura K. Polym J 1982;14:69.
[35] Pope DP, Keller JY. J Polym Sci, Part B: Polym Phys 1976;14:821.
[36] Verma RK, Hsiao BS. Trends Polym Sci 1996;4:312.
[37] Verma RK, Marand H, Hsiao B. Macromolecules 1996;29:7767.
[38] Verma RK, Velikov V, Kander RG, Marand H, Chu B, Hsiao BS. Polymer 1996;37:5357.
[39] Vanderhart DL, Simmons S, Gilman JW. Polymer 1995;36:4223.
[40] Sato T, Okaya T. Polym J 1992;24:849.
[41] Grasruck M, Strobl G. Macromolecules 2003;36:86.
[42] Ivanov DA, Amalou Z, Magonov SN. Macromolecules 2001;34:8944.
[43] Hsiao BS, Sauer BB, Verma RK, Zachmann HG, Seifert S, Chu B, et al. Macromolecules 1995;28:6931.
[44] Jonas AM, Ivanov DA, Yoon DY. Macromolecules 1998;31:5352.
[45] Wang ZG, Hsiao BS, Fu BX, Liu LJ, Yeh I, Sauer BB, et al. Polymer 2000;41:1791.
[46] Chen JC, Chen CC, Wang RC, Fang DM, Tsai M. J Polym 1997;38: 2747.
[47] Crist B. J Polym Sci, Part B: Polym Phys 2001;39:2454.
[48] Crist B. Macromolecules 2003;36:4880.